SATELLITE COLLISION PROBABILITY FOR LONG-TERM ENCOUNTERS AND ARBITRARY PRIMARY SATELLITE SHAPE

Georges Krier[(1)]

[(1)] *SES Engineering, Château de Betzdorf, L-6815 Betzdorf, Luxembourg. Email: georges.krier@ses.com*

ABSTRACT

In this paper we present a nearly approximation-free semi-analytical method to compute the collision probability between two satellites. Unlike the standard methods [1-4], out method does not only perform the three-dimensional integration over the Gaussian position distribution, but also integrates over the three dimensional Gaussian velocity distribution. Our method also overcomes a few other approximations that are sometimes used in the computation of satellite collision probabilities and which are: (a) rectilinear relative motion, (b) small object size compared to the uncertainty of the position and (c) spherical shape of both objects.

1 INTRODUCTION

The aim of this paper is to develop a unified method for collision probability computation that can be applied to all situations where the collision risk of space vehicles needs to be evaluated. In the operational environment at SES where more than 50 geostationary satellites are controlled and monitored, mainly two use cases can be identified:

The first use case is the evaluation of the collision risk of our own satellites with objects like space debris, inactive satellites or upper stages of launch vehicles. In this case the relative velocities are typically high, up to a few km/s, and the encounter times are short, usually not more than a few seconds. Encounters of this type are called short-term encounters in the literature. The orbits of the space debris are determined by JSpOC (Joint Space Operations Center) which tracks more than 20,000 objects down to 10 cm with radar and optical telescopes. If the collision risk is higher than an action threshold, an avoidance manoeuvre will be scheduled in order to reduce the risk below a safety threshold.

The second use case is the design of a colocation strategy and the monitoring of the collision risk of the co-located satellites. SES has a long experience in co-location [9] and grouped up to eight Astra satellites at 19.2°E. In this case the relative velocities are small, typically less than one m/s but the time interval of close approach is long or even permanent. Such events are called long-term encounters in the literature.

2 OVERVIEW

The usual formula for the cumulative collision probability P between two objects (satellites, debris) is found by integrating the three-dimensional Gaussian probability density over the volume V swept by the relative combined hard body of the two objects (see: F.C. Chan's monograph on Spacecraft Collision Probability [7]):

$$P = \iiint_V f(x,y,z)\, dx\, dy\, dz \tag{1}$$

If the positional errors are assumed to be zero-mean, Gaussian and uncorrelated between the two satellites, then the integrant f is the normalized probability density for the 3x3 position covariance matrix C which is the sum of the two individual covariance matrices $C = C_1 + C_2$:

$$f(x,y,z) = \frac{1}{(2\pi)^{\frac{3}{2}}\sqrt{|C|}} e^{-\frac{1}{2}\vec{x}^T C^{-1}\vec{x}} \tag{2}$$

The function f is normalized such that the integral over the entire space equals one.

When the objects are spheres of radius r_1 and r_2, no attitude information is required and the volume V is a tube with a radius equal to the sum of both radii $r = r_1 + r_2$.

Assumptions that are often used are:

- The relative motion is linear during the encounter.
- The covariance matrix is constant during the encounter.
- The objects are spheres.
- The object size is small compared to the error ellipsoid.
- The swept volume is replaced by cylindrical segments.

Several methods were developed in the past to evaluate equation (1) and (2): the first one by Foster [1], used by NASA for debris avoidance operations for the International Space Station (ISS). Improvements and extensions were made by Chan [2, 7], Patera [3] and

Alfano [4, 5, 6]. The work of Coppola [8] is very similar to our approach, it also includes the velocity uncertainty, but only spherical objects are considered, while in our approach the primary object can be of arbitrary convex shape. Therefore the method is well adapted for large space vehicles like the ISS with complex structures larger than the error ellipsoid size.

3 FIRST EXAMPLE

As a boundary case, consider two co-located geostationary satellites where the nominal orbits are in perfect longitude separation and with non-vanishing covariance matrices. The usual formula for the collision probability given in the previous section in equation (1) equals the integral over the tube swept by the relative motion of the combined object and the integrant is the normalized Gaussian probability density. Because the relative velocity is zero, the volume V is empty and hence the collision probability is zero too. What is neglected is the fact that the error ellipsoid is also a dynamical object and when it grows with time it will create also potential collisions, somehow like: "*If the satellite won't come to the error ellipsoid then the error ellipsoid will go to the satellite*". This proves that equation (1) can only be an approximation and that a generalisation is required. This has also been identified by Coppola in [8] where he emphasized the importance to include the velocity uncertainty in the probability computation.

4 THEORY

Instead of computing the collision probability directly, let us first compute the hazard function h which is the collision probability per time unit.

For simplicity assume two objects, a primary satellite of arbitrary shape and with perfectly known orbit (zero covariance matrix) and a secondary object (either another satellite or a debris part) of zero size and arbitrary 6x6 covariance matrix C_6. If both covariance matrices are non-zero the result is the same than for the case where the primary covariance matrix is zero and the secondary covariance matrix equals the sum of both covariance matrices.

The origin of the reference frame is chosen at the centre of gravity of the primary satellite. The secondary is at relative position $\overrightarrow{r_s} = (x_s, y_s, z_s)$ and has relative velocity $\overrightarrow{v_s} = (v_{xs}, v_{ys}, v_{zs})$. Both are grouped in the six dimensional vector $\vec{x}_s$. Take an infinitesimal surface element dA of the primary at position $\overrightarrow{r_A} = (x_A, y_A, z_A)$ with normal vector $\vec{n}$ towards the inside.

It is postulated here that the hazard function dh associated with dA equals the six dimensional integral:

$$dh = dA \int_{\vec{n}\cdot\vec{v}>0} \vec{n}\cdot\vec{v}\;\delta(\vec{r}-\overrightarrow{r_A})\,f_6(\vec{x}-\vec{x}_s)\,dx_{1..6} \qquad (3)$$

The probability that the surface is entered from the opposite direction is obtained by replacing $\vec{n}$ by $-\vec{n}$. The integration vector $\vec{x} = (\vec{r}, \vec{v}) = (x_1..x_6)$ is a six dimensional vector composed of three position and three velocity components and the Dirac delta function $\delta(\cdots)$ imposes $\vec{r} = \overrightarrow{r_A}$. The integrant contains the normalized Gaussian probability density $f_6(\vec{x})$ for the covariance matrix C_6 :

$$f_6(\vec{x}) = \frac{1}{(2\pi)^{\frac{6}{2}}\sqrt{|C_6|}}\, e^{-\frac{1}{2}\vec{x}^T(C_6^{-1})\vec{x}} \qquad (4)$$

For a finite surface element that is not small compared to the error ellipsoid size, an integration needs to be performed over the surface.

Replace the integration variable $\vec{x}$ by $\vec{x}\,' = \vec{x} - \vec{x}_s$ and rename $\vec{x}\,'$ back to $\vec{x}$ .i.e. $\vec{x} \rightarrow \vec{x} + \vec{x}_s$. We then have:

$$dh = dA \int_{\vec{n}\cdot(\vec{v}+\vec{v}_s)>0} \vec{n}\cdot(\vec{v}+\vec{v}_s)\,\delta(\vec{r}+\vec{r}_s-\overrightarrow{r_A})\,f_6(\vec{x})\,dx_{1..6} \qquad (5)$$

We can select the reference system such that the x-axis is in direction of the normal vector $\vec{n}$. Assume that this transformation has already been performed with new $\vec{x}$ and new C_6 . Therefore we have $\vec{n} = \vec{e}_1$ and:

$$\vec{n}\cdot(\vec{v}+\vec{v}_s) = x_4 + v_{xs} \qquad (6)$$

The rotation around $\vec{n}$ can still be freely chosen if required, which will be done at a later stage.

Define D^6 as inverse of C_6 and the hazard function is:

$$dh = \frac{dA}{(2\pi)^{\frac{6}{2}}\sqrt{|C_6|}} \iiint_{-v_{xs},-\infty,-\infty}^{\infty,\infty,\infty} (x_4 + v_{xs}) \cdot exp\left(-\frac{1}{2}\vec{x}^T D^6 \vec{x}\right) dx_{4..6} \qquad (7)$$

where now $x_{1..3}$ are not integration variables anymore but have been defined as:

$$x_1 := x_A - x_s;\;\; x_2 := y_A - y_s;\;\; x_3 := z_A - z_s \qquad (8)$$

The integration over x_6 will be now performed. We will see that its effect is a reduction of the dimension from 6 to 5 without changing the structure of the remaining integral, although the intermediate steps are not trivial.

First group the exponent in powers of x_6:

$$\vec{x}^T D^6 \vec{x} = D^6_{66} x_6^2 + 2\sum_{i=1}^{5} x_i D^6_{i6}\, x_6 + \sum_{i,j=1}^{5} x_i D^6_{ij} x_j \qquad (9)$$

Complete the square:

$$\vec{x}^T D^6 \vec{x} = D^6_{66}\left(x_6 + \frac{\sum_{i=1}^{5} x_i D^6_{i6}}{D^6_{66}}\right)^2 + \sum_{i,j=1}^{5} x_i D^6_{ij} x_j - \frac{\left(\sum_{i=1}^{5} x_i D^6_{i6}\right)^2}{D^6_{66}} \qquad (10)$$

or

$$\vec{x}^T D^6 \vec{x} = D^6_{66}(x_6 + x_c)^2 + \sum_{i,j=1}^{5} x_i D^5_{ij} x_j \qquad (11)$$

where we defined x_c whose value is irrelevant because the integration limits are -∞ to +∞. The new 5x5 matrix D^5 is defined as:

$$D^5_{ij} \stackrel{\text{def}}{=} D^6_{ij} - \frac{D^6_{i6} D^6_{j6}}{D^6_{66}} \qquad (12)$$

and it can be checked in fact that D^5 is the inverse of C_5, the 5×5 submatrix of C_6. In general, let us define C_n as the $n \times n$ submatrix of C_6 and D^n its inverse:

$$D^n = C_n^{-1}; \quad n = 1..6 \qquad (13)$$

The integration from -∞ to +∞ over x_6 is the well-known definite integral over the Gauss function:

$$\int_{-\infty}^{\infty} e^{-\frac{1}{2}D_{66}(\boldsymbol{x_6}-x_c)^2} dx_6 = \frac{\sqrt{2\pi}}{\sqrt{D^6_{66}}} \qquad (14)$$

Therefore one gets:

$$dh = \frac{dA}{(2\pi)^{\frac{5}{2}}\sqrt{|C_5|}} \iint_{-v_{xs}-\infty}^{\infty\,\infty} (x_4 + v_{xs}) \cdot exp\left(-\frac{1}{2}\sum_{i,j=1}^{5} x_i D^5_{ij} x_j\right) dx_{4..5} \qquad (15)$$

using the non-trivial result:

$$|C_6| \cdot D^6_{66} = |C_5| \qquad (16)$$

Thus we have achieved the reduction of the dimension from 6 to 5. Applying the same method for the x_5 integration yields:

$$dh = \frac{dA}{(2\pi)^{\frac{4}{2}}\sqrt{|C_4|}} \int_{-v_{xs}}^{\infty} (x_4 + v_{xs}) \cdot exp\left(-\frac{1}{2}\sum_{i,j=1}^{4} x_i D^4_{ij} x_j\right) dx_4 \qquad (17)$$

The final integral is a bit more complicated because the lower integration limit is $-v_{xs}$ and not -∞ and because of the extra $x_4 + v_{xs}$ factor in front of the exponent. The exponent is grouped again in powers zero, one and two of x_4 and similar to equation (11) we get:

$$\sum_{i,j=1}^{4} x_i D^4_{ij} x_j = D^4_{44}(x_4 + v_b)^2 + \sum_{i,j=1}^{3} x_i D^3_{ij} x_j \qquad (18)$$

where D^4 is the inverse of C_4, the 4x4 submatrix of C_6. With the definition of v_b that has the dimension of a velocity:

$$v_b = \frac{\sum_{i=1}^{3} x_i D^4_{i4}}{D^4_{44}} = \frac{x_1 D^4_{14} + x_2 D^4_{24} + x_3 D^4_{34}}{D^4_{44}} \qquad (19)$$

and with the substitution $x = x_4 + v_b$ and after defining the auxiliaries:

$$\begin{cases} v_c & \stackrel{\text{def}}{=} & v_b - v_{xs} \\ a & \stackrel{\text{def}}{=} & \dfrac{D^4_{44}}{2} \\ \sigma_{vx} & \stackrel{\text{def}}{=} & \dfrac{1}{\sqrt{2a}} \end{cases} \qquad (20)$$

the x_4 dependent part of eq. (17) can be written:

$$\int_{-v_{xs}}^{\infty} (x_4 + v_{xs}) \cdot \exp\left(-\frac{1}{2} D^4_{44}(x_4 + v_b)^2\right) dx_4 \qquad (21)$$

$$= \int_{v_c}^{\infty} x e^{-ax^2} dx - v_c \int_{v_c}^{\infty} e^{-ax^2} dx$$

$$= \frac{e^{-av_c^2}}{2a} - v_c \cdot \frac{\sqrt{\pi}}{2\sqrt{a}} \cdot \left(1 - \text{erf}\left(v_c\sqrt{a}\right)\right)$$

$$= \frac{\sqrt{\pi}}{2a}\left(\frac{e^{-\xi^2}}{\sqrt{\pi}} - \xi \cdot \text{erfc}\ (\xi)\right)$$

where we have defined the dimensionless:

$$\xi \stackrel{\text{def}}{=} v_c\sqrt{a} = \frac{\sigma_{vx}}{\sqrt{2}}(x_1 D_{14}^4 + x_2 D_{24}^4 + x_3 D_{34}^4 - v_{xs} D_{44}^4) \quad (22)$$

Therefore:

$$dh = \frac{dA}{(2\pi)^{\frac{4}{2}}\sqrt{|C_4|}} \cdot exp\left(-\frac{1}{2}\sum_{i,j}^{3} x_i (C_3^{-1})_{ij} x_j\right) \cdot \frac{\sqrt{\pi}}{D_{44}^4}\left(\frac{e^{-\xi^2}}{\sqrt{\pi}} - \xi \cdot \text{erfc}\ (\xi)\right) \quad (23)$$

Using a result similar to eq. (16):

$$|C_4| \cdot D_{44}^4 = |C_3| \quad (24)$$

we get:

$$dh = dA \cdot f_3(\vec{r}) \cdot \frac{\sigma_{vx}}{\sqrt{2}} \cdot \left(\frac{e^{-\xi^2}}{\sqrt{\pi}} - \xi \cdot \text{erfc}(\xi)\right) \quad (25)$$

with the spatial probability density:

$$f_3(\vec{r}) = \frac{1}{(2\pi)^{\frac{3}{2}}\sqrt{|C_3|}} e^{-\frac{1}{2}\vec{r}^T C_3^{-1}\vec{r}} \quad (26)$$

Remember that the x-axis is in direction of the normal vector $\vec{n}$ of the surface element of area dA at $\vec{r}$ which has a spatial probability density function $f_3(\vec{r})$.

For a finite planar surface like a rectangle of a triangle, we have to perform the integral over equation (25):

$$h = \iint_{y,z \in A} f_3(\vec{r}) \frac{\sigma_{vx}}{\sqrt{2}}\left(\frac{e^{-\xi^2}}{\sqrt{\pi}} - \xi\ \text{erfc}(\xi)\right) dy\, dz \quad (27)$$

The integral runs over $y = x_2$ and $z = x_3$ only. The variable $x = x_1$ is constant because we selected the normal vector in x-direction. We still have one degree of freedom to rotate around the x-axis, and this now allows us to set D_{34} equal to zero and thus ξ becomes independent from $z = x_3$ in equation (22). Then the z-integration can be performed analytically and the result is a difference of two error functions. Only the remaining y integration needs to be performed numerically. In order to keep the handling of the integration limits tractable, it is best to choose a simple two dimensional surface and the simplest one is a triangle.

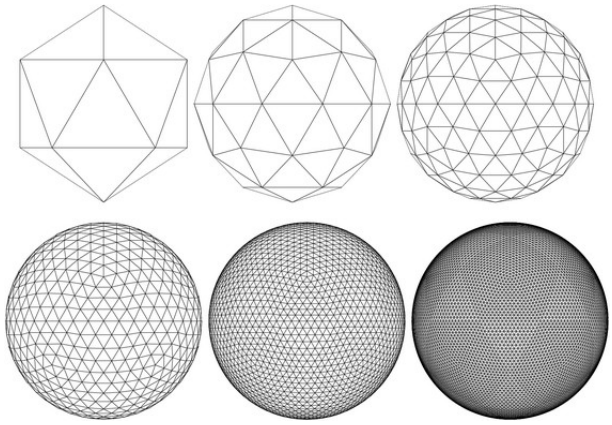

Figure 1: Approximation of a spherical surface by triangles starting from an icosahedron with successive refinements. Shown are approximation of a sphere by icospheres with 20, 80, 320, 1280, 5120 and 20480 triangles (plot from [10]).

Any arbitrary non-planar 3D surface can be split into a finite number of triangles by the triangulation method and for any convex object, the total hazard function is the sum of the contributions of elementary triangles. For non-convex objects, summing up the individual triangle hazard function might result in a too high collision probability because of multiple correlated 'impacts' on aligned structures. Possible shapes are:

- A cuboid (or rectangular parallelepiped or box) for instance has six rectangular faces, each of which can be cut into two triangles, resulting in 12 triangles in total.
- A spherical surface can be approximated by triangles starting from an icosahedron with successive refinements (see figure 1).
- A simple satellite body could be modelled as a box. A solar array can be modelled as a rotating pair of rectangles with opposite normal vectors (not done in this paper).
- Even a complex structure like the ISS can be modelled with finite elements (not done in this paper).

For each elementary triangle, by the choice of the

normal vector, the triangle lies in the y,z plane and the requirement that D_{34} equals to zero uniquely defines the three corners of the triangle (T_1, T_2, T_3) assumed sorted in y. The z-integration is performed analytically and the y-integration by numerical trapezoidal rule. For numerical accuracy reasons we cut the triangle into two triangles (T_1, T_2, T_P) and (T_2, T_P, T_3) where T_P is the projection of T_2 onto the line T_1, T_3 along the z direction (see figure 2). By this choice, the convergence is quadratic instead of only linear with the y step size.

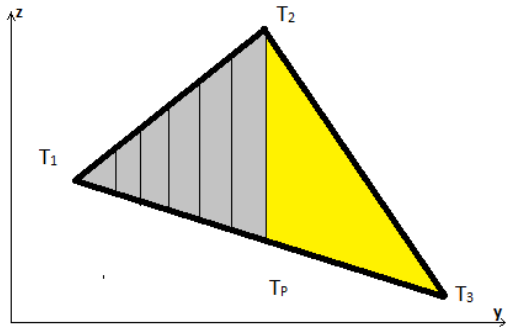

Figure 2. elementary triangle(s) for numerical integration.

We typically need less than 100 terms to reach the wanted accuracy, the number mainly driven by the ratio of the error ellipsoid size over the object size.

In summary one can conclude that the hazard function from such an elementary triangle surface element is a five dimensional integral: a two-dimensional integral over the triangle surface and a three-dimensional integral over the velocity distribution from which, four can be performed analytically, and one must be evaluated numerically.

The total collision probability is the time integral of the hazard function, and this integration is also performed numerically where the step size control is important to find the best compromise between computational performance and numerical accuracy. The time step size is selected to be the maximum of:

- A factor α_1 times the time to reach the minimum of the Mahalanobis distance $\sqrt{\vec{r}^T C_3^{-1} \vec{v}}$ gives Δt_1:

$$\Delta t_1 = \alpha_1 \frac{\vec{r}^T C_3^{-1} \vec{v}}{\vec{v}^T C_3^{-1} \vec{v}} \tag{28}$$

- A factor α_2 times the time to double the square of the Mahalanobis distance from the minimal value gives Δt_2:

$$\Delta t_2 = \alpha_2 \sqrt{\frac{\vec{r}^T C_3^{-1} \vec{r}}{\vec{v}^T C_3^{-1} \vec{v}} - \left(\frac{\vec{r}^T C_3^{-1} \vec{v}}{\vec{v}^T C_3^{-1} \vec{v}}\right)^2} \tag{29}$$

- A factor α_3 times the time to cross the object size plus the uncertainty gives Δt_3:

$$\Delta t_3 = \alpha_3 \cdot \max_{i=1,3} \left(\frac{size_i + \sigma_i}{|v_i|}\right) \tag{30}$$

but never bigger than the "nominal" step size Δt_0.

$$\Delta t_3 = \min\left(\Delta t_0, max(\Delta t_1, \Delta t_2, \Delta t_3)\right) \tag{31}$$

The dimensionless tuning factors $\alpha_{1..3}$ should be smaller than unity, the values used for the comparison were (α_1=0.05, α_2=0.05, α_3=0.02).

The time dependency of the position and velocity covariance matrix can be included without difficulties, and we can use without problems a propagator with a force model including full earth potential, third body perturbations by Sun and Moon, solar radiation pressure and maneuvers.

Implementing this method gives acceptable computation times, such that for long encounters and simple shapes like a cuboid, the collision probability evaluation requires CPU time in the order of 10 ms, which is less than for a typical orbit and covariance propagation. For more complex shapes, like an icosahedron composed of about 20000 triangles, the CPU time is in the order of 10 s.

So far, we have assumed that the secondary object is a point of zero size. If the secondary object is a debris part, it is usually modelled as sphere because we do not know its attitude or its behavior over time. It is probably rotating and tumbling and we can only approximate it as a sphere with an effective cross-section *r*. Then we we can still assume zero size for it, but the primary object will be replaced by a combined hard body which is the primary 'inflated' in each direction by *r*; a sphere of radius R becomes a sphere of radius $R + r$; a box becomes a 'box with rounded edges' that can be approximated by a box where each side is increased by $2r$. For two co-located satellites with aligned spatial orientation and modelled as boxes, the combined hard body volume is again a box where each side length is the sum of the individual size lengths.

5 VALIDATION

5.1 Comparison with literature test cases

As validation we use the first eight test cases created by S. Alfano in [6] where he runs Monte Carlo (MC) simulations with pure Keplerian propagation of the state vector and the associated covariance. Case 1 to 4 describe the relative motion for two satellites in geosynchronous orbits (GEO), case 5 to 7 are two low earth orbits (LEO) and the last one two mid-earth orbits (MEO).

Unfortunately all test cases objects are spheres, not a single one is a box. Therefore, in order to reach a sufficiently good numerical match with the reference, we replace the sphere as a subdivided icosahedron composed of 81920 triangles. Such a large number is not as efficient as the method described in [8], but we just use them exceptionally for the validation of the method, while for operational use, the primary is usually modelled as box.

The results are shown in table 1. For all test cases our method is able to match the MC results of [6] with a typical difference of 0.6%, unlike other semi-analytical methods [1-4] which give only approximate results. Coppola [8] ran test cases 4 and 8 and is also able to reproduce the MC results.

5.2 Comparison with Monte Carlo simulation

In parallel to the analytical computation, a Monte Carlo simulator as independent validation was set up, also in view of non-spherical objects for which no test cases were found in the literature.

Monte Carlo can be considered as the gold standard for collision probability validations because the method is mathematically simple; you merely need a propagator and need to detect collisions. It might be too slow for operational use, but for a validation run a few minutes or hours of CPU time is affordable.

In each run, we add to both state vectors random errors using a Cholesky decomposition of the covariance matrix. The state vector is propagated by freezing the first five Kepler elements and the true anomaly is obtained from the time using Kepler's equation. A variable step size is used to detect the collision, which is the entry of the secondary, modelled as point mass, into the primary, which in the current MC implementation can be either a sphere or a box.

The monitoring interval can be reduced to the time interval where the analytical hazard function is non-vanishing. For the comparison with the analytical computation, violations present already at the initial epoch are disregarded because the entry happened before. Multiple violations in a single MC run should be counted each, but they did only occur for test case 8 with a probability of $1 \cdot 10^{-8}$. For each test case, $N=7 \cdot 10^{8}$ runs were performed. With a collision probability of p for a single event, the standard deviation of the MC probability is:

$$\sigma = \sqrt{\frac{p \cdot (1-p)}{N}} \qquad (32)$$

The results are shown in the last column of table 1 and can be compared to the analytical results and to the MC results from [6]. The match with the former is good with an average difference of 0.1% which is a bit more than the MC standard deviation especially for case #6. Reasons for this larger difference could be the icosphere approximation, the finite time step size, the discrete numerical y-integration, the different orbit integrator (numerical vs. usage of Kepler equation).

	Obj. size	Rel. vel. at TCA	collision probability		
#	m	(m/s)	analytical	Monte Carlo [6]	Monte Carlo
1	15	0.01	**0.216801**	**0.217**467	**0.216818** ± 0.000016
2	4	0.01	**0.01555**8	**0.01573**7	**0.015569** ± 0.000005
3	15	16	**0.10034**7	**0.10084**6	**0.100346** ± 0.000011
4	15	0.02	**0.07363**3	**0.07309**0	**0.0736337** ± 0.000010
5	10	0.5	**0.04448**9	**0.04449**9	**0.044504** ± 0.000008
6	10	0.2	**0.00431**7	**0.00430**1	**0.004334** ± 0.000002
7	10	0.2	**0.0001616**	**0.0001615**	**0.0001615** ± 0.0000005
8	4	0.001	**0.03524**9	**0.03525**6	**0.035239** ± 0.000007

Table 1. Comparison of analytical results with MC runs of Alfano [6] and with our own MC runs. Matching digits are displayed in bold blue.

The hazard function which is the rate of collisions per time interval is displayed for test case 1 in figure 3, and shows a very good match between the analytical computation and the MC simulation.

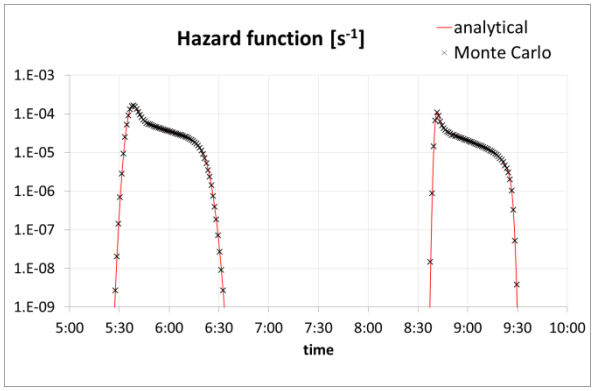

Figure 3: hazard function for test case 1. The collision risk is highest between 5:30 and 6:30 s and between 8:40 and 9:30 s. The solid red line is the analytical result, and the MC result are displayed as black crosses.

6 TEST CASES FOR BOX SHAPED OBJECTS

We present here three test cases for non-spherical objects. Table 2 summarizes the collision probability obtained by the analytical method and by Monte Carlo

simulation with $7 \cdot 10^8$ runs. The match is good, with an average difference of 0.2% but larger than the MC standard deviation.

It is assumed that the attitudes of the satellites are aligned with their respective orbital frames.

case	Primary and secondary size (m)	Collision probability	
		analytical	Monte Carlo
A	5x5x5 5x5x5	**0.012**866	**0.012**851 ±0.000004
B	20x20x20 Point mass	**0.204**266	**0.204**096 ±0.000015
C	3x2x4 Point mass	**0.133**152	**0.132**902 ±0.000013

Table 2: Collision probabilities for rectangular cuboids. Matching digits are displayed in bold blue.

6.1 Case A: zero relative velocity.

Here we consider the example mentioned in section 3 with two geostationary satellites separated *100 m* tangentially and with zero relative velocity for their nominal orbits for which the "classical" collision probability equation gives zero.

The combined covariance is diagonal with radial, tangential, normal (RTN) position uncertainties of (*1, 1, 1*) *m* and RTN velocity uncertainty of (*0.01000, 0.01414, 0.00141*) *m/s* (all data specified in appendix A). The satellites bodies are modelled as cubes with a side length of 5 m. Assuming that their attitudes are aligned (because their orbits are nearly identical), this is equivalent to a combined cubic object size of *10 x 10 x 10 m*. The monitoring interval is one orbital period i.e. one sidereal day.

The hazard function is displayed in figure 4, differentiated per face plus the sum of them. It starts from a low value at the initial epoch because of the initial guaranteed tangential separation of *100 ± 1 m,* but then the velocity uncertainty makes the East face risk grow fast to reach a maximum of about $2 \cdot e^{-6}$ s^{-1} around 01:00 later and to fall below $1 \cdot 10^{-10}$ s^{-1} around 14:00. The risk for the Anti Earth face varies in a similar way, while the others faces contribute less and later to the overall risk. For low values of the hazard function, one might note the increasing numerical noise of the MC hazard function, because only a few events are found in the corresponding time bins of five minutes.

The total collision probability is 0.012868 for the analytical method compared to 0.012851 for the MC computation.

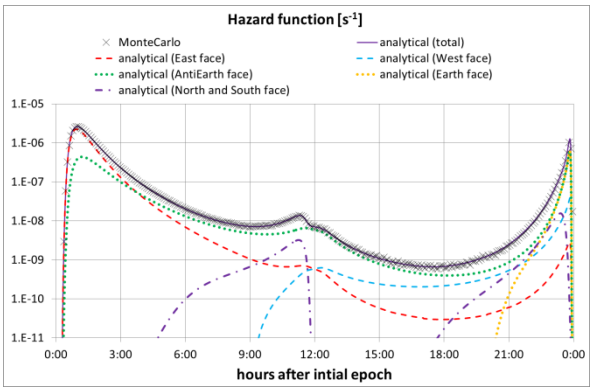

Figure 4: hazard function of two geostationary satellites differentiated per face (coloured lines) and summed up (solid black line) and which matches well the Monte Carlo result (black crosses).

6.2 Case B: long-term encounter

Here we use the same orbit than test case 1 of [6] (see figure 3) but with different object shape and slightly different covariance. The miss distance of about *5 m* is less than the combined object size of *20 x 20 x 20 m* and the of same order of magnitude than the radial, tangential and normal position uncertainty of (*2, 80, 2*) *m*. Figure 5 shows the hazard function over one hour covering the first peak. Four faces contribute to the collision risk, mainly the Earth face then later East face, small risk for North and South face and no risk for the West face and Anti-Earth face.

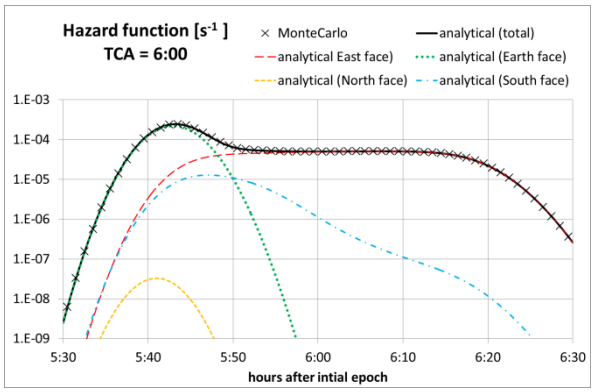

Figure 5: hazard function for case B differentiated per face (coloured lines) and summed up (solid black line) confirmed by Monte Carlo (black crosses).

6.3 Case C: short-term encounter with higher relative velocity.

This case validates the method for a short encounter with higher relative velocity, for which in principle equation (1) could be used and where the time integration could be performed analytically. The aim is to demonstrate that the time step choice described by eq. (28) to (31) produces sufficiently precise results.

Let us consider a box shaped primary geostationary satellite of *3x2x4 m* and a secondary point mass. The closest relative RTN position is *(2,2,2) m*, with a relative RTN velocity of *(100,-100, 100) m/s* and a RTN position uncertainties of *(1,2,3) m*.

The hazard function shown in figure 6 is nonzero only in a 0.2 second time interval. Only the Earth-, East and South face can be hit. In general the hazard function peaks are earlier than the time of closest approach (of the center of gravity) because of the finite size of the primary. In this example the Monte Carlo simulation also differentiates per face.

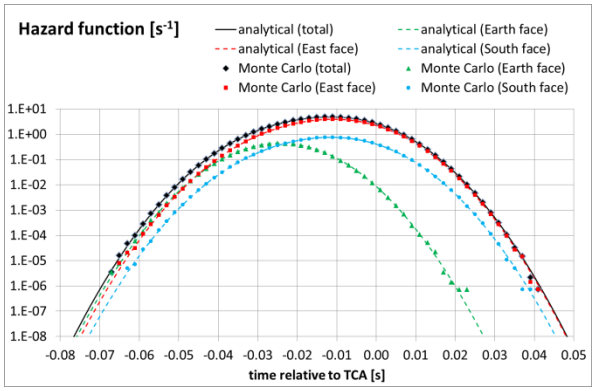

Figure 6: analytical and Monte Carlo hazard function for case C (large relative velocity) differentiated per face.

7 CONCLUSION

As a conclusion we obtain a method that is nearly approximation-free, computationally fast and that can be used in the day-to-day close approach monitoring of the SES fleet. It can be applied for short and long term encounters, for any satellite shape and it does not only give the total collision probability, but also the instantaneous hazard function.

The method has been successfully validated against Monte Carlo simulations to sub percent accuracy.

8 REFERENCES

1. Foster, J. L., & Estes, H. S. (1992). A parametric analysis of orbital debris collision probability and maneuver rate for space vehicles. *NASA JSC*, *25898*.
2. Chan, K. (1997). Collision probability analysis for earth orbiting satellites. *Space cooperation into the 21 st century*, 1033-1048.
3. Patera, R. P. (2001). General method for calculating satellite collision probability. *Journal of Guidance, Control, and Dynamics*, *24*(4), 716-722.
4. Alfano, S. (2005). A numerical implementation of spherical object collision probability. *Journal of the Astronautical Sciences*, *53*(1), 103.
5. Alfano, S. (2007, August). Beta conjunction analysis tool. In *AAS/AIAA Astrodynamics Specialist Conference, Mackinac Island, MI., Paper* (pp. 07-393).
6. Alfano, S. (2009). Satellite conjunction monte carlo analysis. *AAS Spaceflight Mechanics Mtg, Pittsburgh, PA., Paper*, 09-233.
7. Chan, F. K. (2008). *Spacecraft collision probability* (pp. 1-12). El Segundo, CA: Aerospace Press.
8. Coppola, V.T., "Including velocity uncertainty in the probability of collision between space objects," AAS/AIAA Space Flight Mechanics Meeting, Charleston, SC, 2012.
9. Wauthier, P., Francken, P., & Laroche, H. (1997, August). Co-location of six ASTRA satellites: Assessment after one year of operations. In *Space Flight Dynamics* (Vol. 403, p. 13).
10. Satoh, et al. (2014). The non-hydrostatic icosahedral atmospheric model: Description and development. *Progress in Earth and Planetary Science*, *1*(1), 18.

Appendix A: test cases

Case 1..8 can be found in [6]

Case A:

```
PRIMARY_SIZE_3D=5 5 5 m
PRIMARY_EPOCH=01-Mar-2016:00:00:00
PRIMARY_POSITION=42164170.3 0 0 m
PRIMARY_VELOCITY=0 3074.6600525 0 m/s
PRIMARY_COVARIANCE=36*0
SECONDARY_SIZE_3D=5 5 5 m
SECONDARY_EPOCH=01-Mar-2016:00:00:00
SECONDARY_POSITION=42164170.3 100 0 m
SECONDARY_VELOCITY=-0.0072921151467064 3074.6600525 0.0
SECONDARY_COVARIANCE=DIAG(1,1,1,0.0001, 0.0002, 0.000002) m^2,..m^2/s^2
START=01-Mar-2016:00:00:00  END=01-Mar-2016:23:56:04
```

Case B:

```
PRIMARY_SIZE_3D=20 20 20
PRIMARY_EPOCH=04-Mar-2016:06:00:00
PRIMARY_POSITION= 153446.7645602800 41874155.8695660000  0.0000000000
PRIMARY_VELOCITY= 3066.8747609105    -11.3736149565  0.0000000000
PRIMARY_COVARIANCE=36*0
SECONDARY_SIZE_3D=0 0 0
SECONDARY_EPOCH=04-Mar-2016:06:00:00
SECONDARY_POSITION=153447.2642029000 41874156.3699030000  4.9999660258
SECONDARY_VELOCITY=3066.8647607073    -11.3636148179  -0.0000013581
SECONDARY_COVARIANCE=
6494.224931854500000000000 -376.156116653730000000000 -0.000044917291988265000
  0.015992172760904000000  -0.494272101759260000000 -0.000000059018359337438

-376.156116653730000000000   25.000000000000000000000  0.000025501472714422000
 -0.000988464580979650000   0.028570758726652000000  0.000000034189216426795

  -0.000044917291988265000    0.000025501472714422000  4.000000000000000000000
 -0.000000001180334503685   0.000000034189216426795 -0.000060715345613191000

   0.015992172760904000000   -0.000988464580979650000 -0.000000001180334503685
  0.000000044383012786732 0  -0.000012124371638594000 -0.000000000001447705672

  -0.494272101759260000000    0.028570758726652000000  0.000000034189216426795
 -0.000012124371638594000   0.000037623723352821000  0.000000000044920403553

  -0.000000059018359337438    0.000000003418729542731 -0.000060715345613191000
 -0.000000000001447705672   0.000000000044920403553  0.000010000000000000000

START=04-Mar-2016:05:30:00    END=04-Mar-2016:06:30:00
```

Case C:

```
PRIMARY_SIZE_3D=3 2 4
PRIMARY_EPOCH=01-Apr-2017:00:00:01
PRIMARY_POSITION=42164170 0 0
PRIMARY_VELOCITY=0 3074.66 0
PRIMARY_COVARIANCE=36*0
SECONDARY_SIZE_3D=0 0 0
SECONDARY_EPOCH=01-Apr-2017:00:00:01
SECONDARY_POSITION=  42164172 2 2
SECONDARY_VELOCITY= 100 2974.66  100
SECONDARY_COVARIANCE=DIAG(1,4,9,0.01,0.01,0.01)
START=01-Apr-2017:00:00:00.8 END=01-Apr-2017:00:00:01.2
```